Heterogeneous & Homogeneous & Bio- & Nano-

CHEMCATCHEM

CATALYSIS

Accepted Article

Title: Baeyer-Villiger oxidation of cyclic ketones using tin-silica pillared catalysts

Authors: Jan Prech, Marta Arroyo Carretero, and Jiří Čejka

To be cited as: *ChemCatChem* 10.1002/cctc.201700162

Link to VoR: http://dx.doi.org/10.1002/cctc.201700162

A Journal of ChemPubSoc Europe

WILEY-VCH

www.chemcatchem.org

Baeyer-Villiger oxidation of cyclic ketones using tin-silica pillared catalysts

Jan Přech*[a], Marta Arroyo Carretero[a], Jiří Čejka[a]

Abstract: Baeyer-Villiger oxidation is an important transformation of ketones into esters and particularly cyclic ketones to lactones. We report here preparation and catalytic activity of layered Sn-silicate catalysts and mesoporous ordered silica catalysts in this reaction. Sn was introduced using so-called tin-silica pillaring or impregnation using a mixture of tetraethyl orthosilicate and tin (IV) alkoxide. The prepared catalysts were characterized using XRD, N_2 physisorption, SEM, UV/Vis, and ICP-OES and studied in Baeyer-Villiger oxidation of cyclopentanone, norcamphor, and 2-adamantanone with aqueous hydrogen peroxide. Norcamphor and 2-adamantanone were oxidized easily with selectivity up to 99%. Sn-MS and IPC-1-SnPI materials exhibited the highest conversions (e.g. norcamphor: Sn-MS 37%, IPC-1-SnPI 36% after 8 h vs. Sn-MCM-41 22%). On the other hand, oxidation of cyclopentanone suffered from product hydrolysis to corresponding 4-hydroxybutanoic acid.

Introduction

Baeyer-Villiger oxidation was firstly reported by Adolf Baeyer and Victor Villiger[1] as a direct conversion of ketones into esters and lactones by reaction with a peroxo specie. This reaction has been widely used in synthetic organic chemistry particularly in preparation of natural products (e.g. antibiotics, steroids, pheromones), in synthesis of fragrances, flavors or monomers for polymerization. [2]

The mechanism of Baeyer-Villiger reaction proposed by Criegee[3] consists of two steps. First, the peroxide specie (acting as a nucleophile) attacks the carbonyl group of the ketone giving an sp^3 specie. Second, the sp^3 specie converts to ester by migration of one of the adjacent carbons to oxygen.

Typically, peracids (e.g. trifluoroperoxyacetic acid) or persulfate salts (e.g. potassium monopersulfate) are employed as the peroxo species. Their use, however, shows several disadvantages such as safety issues, bad mass economy (obtaining carboxylic acid or salt as a side product)[4] and the necessity of strong acids in the reaction media due to a low reactivity of the peracids in particular reactions. [5] The mentioned disadvantages of peracids have promoted intensive search for new catalysts active with simple oxidants such as hydrogen peroxide. [6] Catalysts based on molecular sieves modified with tin (e.g. Sn-**BEA**, Sn-MCM-41) or germanium (e.g. **UTL**, ITQ-17), have showed excellent selectivity in the Baeyer-Villiger oxidation of cyclic ketones with H_2O_2 as oxidant. [7]

In a number of reactions (e.g. epoxidation, sulphoxidation), zeolite-based catalyst (e.g. TS-1) activate the hydrogen peroxide. However, Sn-silicalite catalysts are highly selective in Baeyer-Villiger oxidation, because their Sn Lewis acid sites activate carbonyl groups and subsequently utilize non-activated hydrogen peroxide. [8]

Ordered mesoporous silica based catalysts (e.g. Sn-MCM-41) can be prepared either by direct synthesis or tin can be incorporated by means of post-synthesis modification and there is a little difference in their Lewis acidity and catalytic properties [7c]. Nevertheless, for oxidation of 2-adamantanone (a sterically demanding substrate), Sn-**BEA** was found the most active catalyst (e.g. turn-over frequency in 1 h: Sn-**BEA** 210 h^{-1}, Sn-MCM-41 58 h^{-1} Sn-**MFI**-nanosheets 38 h^{-1}). [9] Taking into account promising results obtained with the Sn-**BEA** zeolite catalyst on one hand and considering pore-diffusion limitations, characteristic for conventional zeolites on the other hand, [10] Sn-containing hierarchical or lamellar materials could be the effective catalysts for oxidation of bulky ketones. Highlighting the role of diffusion in the tin-zeolite catalysed, Conrad et al. [11] studied kinetics of Baeyer-Villiger oxidation of cyclohexanenone over Sn-**BEA** (Si/Sn molar ratio 217) showing that the reaction occur in kinetic regime only at temperature below 65°C under the used conditions and also hydrophillicity of the material influences the reaction.

Recently, Al-Nayili et al. [12] prepared hierarchical Sn-**BEA** for Meerwein-Ponndorf-Verley transfer hydrogenation showing its advantage in higher resistance towards deactivation in comparison with conventional Sn-**BEA**.

Lamellar zeolites possess higher external surface areas in comparison with conventional ones. The external surface is well accessible even for sterically demanding molecules. Therefore, a lamellar material should exhibit an increased catalytic activity in comparison with a conventional zeolite, thanks to the improved accessibility of the active sites. [10a, 13] In this way, Sn containing **MFI** nanosheets have been prepared and tested in the Baeyer-Villiger oxidation of bulky cyclic ketones. Luo et al. [9] reported direct synthesis of Sn-**MFI** nanosheets using an amphiphilic organic structure directing agent. The Sn-**MFI** nanosheets were active in Baeyer-Villiger oxidation of 2-adamantanone and clearly exhibited an increased activity in comparison with conventional Sn-**MFI** (e.g. TOF (Sn-**MFI** nanosheets) = 38 h^{-1} vs. TOF (Sn-**MFI**) = 5 h^{-1}). However, these results do not represent a considerable improvement in comparison with Sn-**BEA** and Sn-MCM-41. Ren et al. [14] prepared and tested self-pillared Sn-**MFI** in glucose and lactose isomerization. The lamellar character of the material resulted in an improved conversion and selectivity compared with micro- and mesoporous catalysts (Sn-**BEA** and Sn-MCM-41).

Recently, our group reported so-called silica-titania pillaring of layered silicates and titanosilicates. [10c, 15] The use of silica-titania pillared catalysts led to a substantial improvement of the conversion in epoxidation reactions in comparison with layered and pure silica pillared materials. This method enables to prepare an active epoxidation catalyst from a lamellar zeolite, which does not possess any titanium incorporated via direct

---

[a] Dr. J. Přech, M. Arroyo Carretero, Prof. Dr. J. Čejka.
Department of Synthesis and Catalysis
J. Heyrovský Institute of Physical Chemistry, Academy of Sciences of the Czech Republic, v.v.i.,
Dolejškova 2155/3, CZ-182 23 Prague 8, Czech Republic
Phone: +420 266 053 856
E-mail: jan.prech@jh-inst.cas.cz

synthesis. Encouraged by these results, we examined this approach in the preparation of tin-silica pillared catalysts.

In this contribution, we report the synthesis and catalytic investigation of tin-silica pillared materials and impregnated layered materials with **MFI** and **UTL** topology of their crystalline layers. For comparison, Sn-SBA-15 and Sn-SBA-16 materials were prepared by impregnation method while a new amorphous mesoporous tin-silicalite (denoted Sn-MS) was obtained by direct synthesis. Sn-MCM-41 and Sn-**BEA** were used as benchmarking materials. All catalysts were studied in Baeyer-Villiger oxidation of bulky cyclic ketones (2-adamantanone, norcamphor) and cyclopentanone. Layered **MFI** zeolites were prepared as pure silica according to the Ryoo protocol[10b] and impregnated with tin precursors to obtain Sn-lam-**MFI** catalysts. Tin-silica pillaring of the pure-silica layered **MFI** under various conditions was used to prepare **MFI**-SnPI. In the same way, IPC-1P layers, obtained by top-down transformation of zeolite **UTL,** [16] led to IPC-1-SnPI.

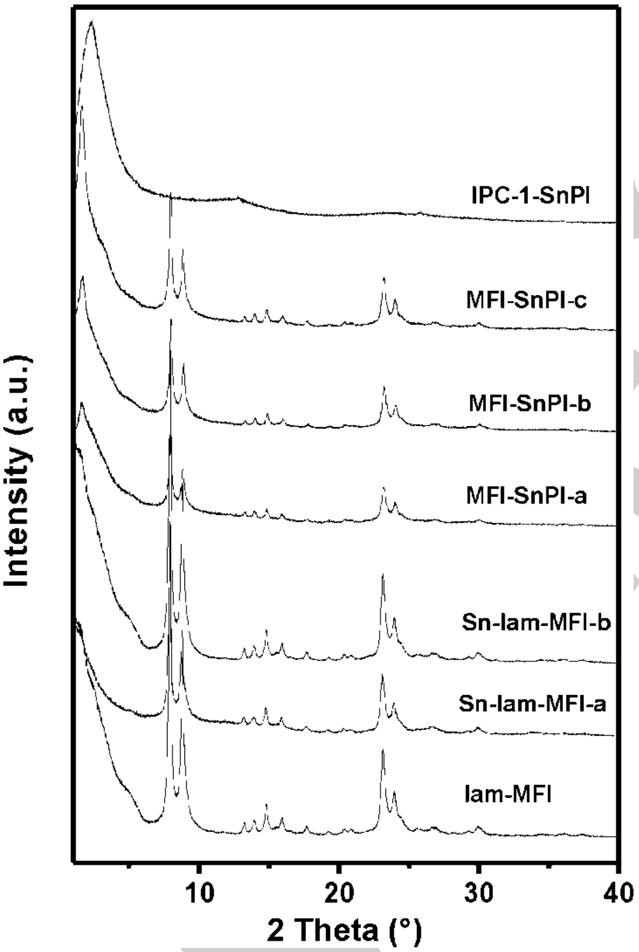

Figure 1. Powder XRD patterns of tin layered zeolite catalysts.

Results and Discussion

Material characterization

A group of tin-silica pillared **MFI** catalysts (**MFI**-SnPI-a, **MFI**-SnPI-b, **MFI**-SnPI-c) and a group of impregnated lamellar **MFI** catalysts (Sn-lam-**MFI**-a, Sn-lam-**MFI**-b) have been prepared from a parent all-silica lamellar **MFI** material (lam-**MFI**). The impregnated lam-**MFI** catalysts consist of Sn impregnated **MFI** layers of approximately 2 nm thickness. [17] The pillared catalysts consist of the **MFI** layers, which are kept apart by amorphous pillars of Sn-containing silica. [18] In other words, the interlayer space is partly filled with amorphous mesoporous tin-silica phase. The IPC-1-SnPI material consists of crystalline silica layers formed by disassembly of **UTL** zeolite[15-16, 18] and Sn-containing silica pillars like in the case of **MFI**-SnPI catalysts.

Figure 1 shows powder XRD patterns of samples with crystalline zeolite layers after calcination. The XRD patterns of lam-**MFI** parent material and all the **MFI** based tin containing catalysts are consistent with the patterns of nanosheet **MFI** and TS-1. [10b, 17] The pillared materials exhibit one intensive diffraction line at approximately 2θ=1.7° while in the patterns of parent lam-**MFI** and impregnated Sn-lam-**MFI** materials this line is not present. This line corresponds to an average distance between layers, which are supported by the tin-silica pillars and also indicates their regularity. [10b, 10c, 20] The crystalline layers in the lam-**MFI** and Sn- lam-**MFI** samples are randomly oriented one on another No changes in the XRD patters were observed upon Sn impregnation (Figure 1). Therefore, the incorporation of Sn by impregnation did not influence the structure of the crystalline layers as evidenced in the samples Sn-lam-**MFI**-a and Sn-lam-**MFI**-b.

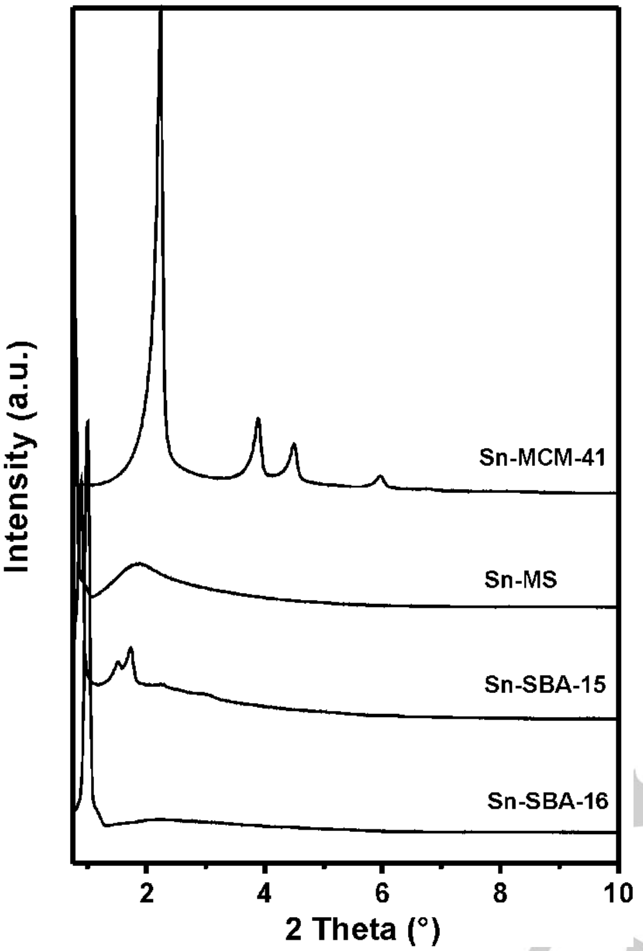

Figure 2. XRD patterns of tin containing ordered mesoporous silica catalysts.

During IPC-1-SnPI preparation by hydrolysis of the **UTL**, [15-16] most of the diffraction lines disappeared due to the structure disassembly. The most intensive diffraction line in IPC-1-SnPI pattern is detected at 2θ 2.3°, which corresponds to d-spacing 3.8 nm (characteristic for pillared IPC-1PI materials). [16]

Low-angle XRD patterns of ordered mesoporous tin-silica catalysts are presented in Figure 2. Sn-MCM-41 exhibits the characteristic diffraction lines of MCM-41 materials with reflections corresponding to (100), (110) and (200) planes, indicating a well-defined 2D hexagonal mesostructures. [21] The Sn-SBA-15 exhibits a well-resolved diffraction pattern with a prominent peak at 2θ=0.9° and other two peaks at 2θ=1.65 and 1.85° characteristics of the purely siliceous SBA-15. [22] Sn-SBA-16 displays only one intensive peak at 2θ=0.99° corresponding to polyhedral particles and indexed by plane (110), [23] however the shape of the nitrogen sorption isotherm (*vide infra*) is clearly consistent with the SBA-16 structure.

The XRD pattern of Sn-MS material contains only two diffraction lines at 2θ=0.76° and 2θ=1.75° (clearly observable in Figure S4, supporting information). Therefore, we conclude it is amorphous. Nevertheless, the mentioned diffraction lines may point to some sort of organisation similar to ordered mesoporous silica materials (e.g. SBA-15, SBA-16). [22] The position of the second line (1.75°) also corresponds to the interlamellar distance in lam-**MFI** (synthesized in the presence of the same organic surfactant) and also the 0.75° line is very sharp and intensive, therefore another possible explanation is a layered character of the material. XRD pattern for Sn-**BEA** reference synthetised according to Renz et al. [7b] is presented in Figure S1.

SEM images of representative catalysts are given in Figure 3. The pillared samples **MFI**-SnPI-a and **MFI**-SnPI-b consist of flake-like crystals forming agglomerates with a size of about 5-10 µm. The IPC-1-SnPI material has a morphology of thin-plate crystals, which is similar to the initial **UTL** morphology, despite the post-synthesis modifications including materials disassembly into layers. Sn-SBA-16 exhibits rounded shape particles with size between 2-6 µm, typical for this kind of materials. The catalyst Sn-MS shows a peculiar sponge-like morphology with visible macropores.

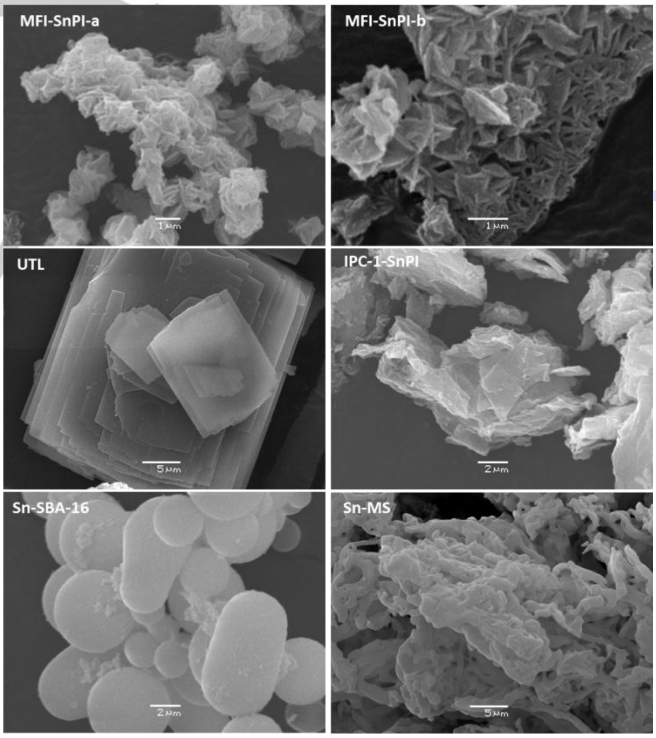

Figure 3. SEM images of selected discussed materials.

Table 1. Textural properties, tin content and way of preparation of the discussed catalysts.

Catalyst	Tin precursor	Tin incorporation method	Si/Sn	S_{BET} (m^2/g)	S_{ext} (m^2/g)	V_{tot} (cm^3/g)	V_{mic} (cm^3/g)
lam-MFI	--	--	--	474	190	0.39	0.13
Sn-lam-MFI-a	$Sn(OBu)_4$	Impregnation	156	460	160	0.37	0.11
Sn-lam-MFI-b	$SnCl_4$	Impregnation	27	377	143	0.29	0.11
MFI-SnPI-a	$Sn(OBu)_4$	Pillaring	19	547	263	0.35	0.13
MFI-SnPI-b	$Sn(OCH(CH_3)_2)_4$	Pillaring	30	492	228	0.32	0.12
MFI-SnPI-c	$Sn(OCH(CH_3)_2)_4$	Pillaring	44	596	362	0.37	0.10
IPC-1-SnPI	$Sn(OBu)_4$	Pillaring	32	790	66	0.41	0.16
Sn-SBA-16	$SnCl_4$	Impregnation	53	817	41	0.60	0.07
Sn-SBA-15	$SnCl_4$	Impregnation	41	693	74	1.10	0.03
Sn-MS	$SnCl_4 \cdot 5H_2O$	Direct synthesis	17	920	117	1.17	0
Sn-MCM-41	$SnCl_4$	Impregnation	50	1256	119	1.01	0
Sn-BEA	$SnCl_4 \cdot 5H_2O$	Direct synthesis	220	538	28	0.26	0.22

Textural properties and tin content of the catalysts under study are listed in Table 1 together with details on tin incorporation. The incorporation of tin by impregnation resulted in a decrease in the BET area and total pore volume with respect to the parent material. The impregnation with $SnCl_4$ solution led to a higher Sn content (Sn-lam-**MFI**-b, Si/Sn = 27) in comparison with tin(IV) butoxide impregnation (Sn-lam-**MFI**-a Si/Sn = 156). On the other hand, lower BET area (377 m^2/g) and total pore volume (0.29 cm^3/g) were observed for Sn-lam-**MFI**-b in comparison with Sn-lam-**MFI**-a (S_{BET}=460 m^2/g and V_{tot}= 0.37 cm^3/g). The micropore volume as well as external surface area only slightly decreased upon impregnation (V_{mic}: 0.11 cm^3/g (Sn-lam-**MFI**-a,b) vs. 0.13 cm^3/g (lam-**MFI**), S_{ext}: 160 m^2/g (Sn-lam-**MFI**-a), 143 m^2/g (Sn-lam-**MFI**-b) vs. 190 m^2/g (lam-**MFI**)). This indicates that both $SnCl_4$ and $Sn(OBu)_4$ penetrate with difficulties into the **MFI** micropores and therefore, preferential impregnation of the external surface of the layers is expected.

Incorporation of tin by pillaring method led to preservation of the total adsorption capacity even if the Si/Sn ratio was below 30. The presence of the pillars between the layers keeps the structure more open. The highest BET area (596 m^2/g) and total adsorption volume (0.37 cm^3/g) were achieved for the sample **MFI**-SnPI-c containing Si/Sn ratio 44. Also the external surface area of this material is almost two times higher (362 m^2/g) in comparison with parent lam-MFI (190 m^2/g).

The IPC-1-SnPI catalyst shows the highest BET area (790 m^2/g) and total adsorption capacity (0.41 cm^3/g). Interestingly, the material exhibits micropores (Vmic = 0.16 cm^3/g), although similar purely siliceous material is purely mesoporous. [15-16] Most probably this is because tin precursor in the pillaring medium causes formation of thicker pillars and therefore narrower pores in between. The shape of the isotherms of the pillared samples is typical, expressing an increase in the range approximately p/p_0 = 0.05 – 0.3 (Figure 4). This increase corresponds to filling of mesopores in between the layers, which belong to lower mesopores region.

BET areas of the mesoporous molecular sieves are generally higher than those of lamellar samples (693-1256 m^2/g). The highest S_{BET} and total pore volume correspond to Sn-MCM-41 (Table 1). The N_2 sorption isotherms for Sn-MCM-41, Sn-SBA-15, and Sn-SBA-16 are characteristic for the MCM-41, SBA-15, and SBA-16 materials, respectively. The hysteresis loop of the Sn-SBA-15 material is typical for parallel cylindrical pores and while in the Sn-SBA-16 corresponds to cage-like mesoporous materials [24]. The sample Sn-MS displayed a IUPAC type IV isotherm with H2 hysteresis loop, which is characteristic for mesoporous materials with interconnected pore geometry [24]. It exhibited BET area 920 m^2/g and total adsorption volume 1.17 cm^3/g without any micropores. Reference Sn-**BEA** catalyst exhibited IUPAC type I isotherm (typical for microporous material and textural properties (BET= 538 m^2/g, V_{mic} = 0.22 cm^3/g) consistent with the source reference. [7b] The nitrogen sorption isotherm (Figure S2) and SEM image (Figure S3) are presented in the supporting information.

Because the starting materials for impregnation and tin-silica pillaring did not contain any tin, the Sn sites are expected to be located mainly on the outer surface of the layers and on the surface of silica pillars in the case of lamellar samples. The Sn-alkoxides used for the impregnation and pillaring are sterically demanding and therefore deep penetration into MFI micropores inside the layers is not expected. On the other hand, for the ordered mesoporous silica materials, no diffusion restrictions for the Sn source and therefore homogenous Sn distribution on the surface are assumed.

DR-UV/Vis spectroscopy technique was employed to determine the state of Sn in the catalysts. The spectra were collected on calcined samples. Especially the presence of isolated 4-coordinated Sn species is important to achieve a high catalytic activity in the Baeyer-Villiger reaction. [7b] These species exhibit a characteristic absorption band at ~205 nm. [25] Bulk SnO_2 phase, which is inactive for the oxidation catalysis, absorbs at approximately 280 nm [26] (Figure 5). The materials prepared using pillaring method (**MFI**-SnPI-a, **MFI**-SnPI-b, **MFI**-SnPI-c, IPC-1-SnPI) contain mostly isolated 4-coordinated tin atoms. Similarly $Sn(OBu)_4$ impregnated Sn-lam-MFI-a contains mostly these species, while in the material prepared using $SnCl_4$ (Sn-lam-**MFI**-b) an intensive band centred at 270 nm indicates a presence of SnO_2.

The UV-Vis spectra of Sn-MS, Sn-SBA-16, and Sn-SBA-15 were qualitatively similar to those of tin-silica pillared samples, indicating mostly presence of isolated 4-coordinated tin species (characteristic absorption ~205 nm). The catalyst Sn-MCM-41 showed a broad band centred at approx. 230 nm. The signal at 230 nm has been assigned previously to isolated 6-coordinated species. [27] Similarly the Sn-**BEA** catalyst exhibited two bands at approx. 210 nm and 250 nm assigned to isolated 4- and 6-coordinated Sn species.

Acidic properties of **MFI**-SnPI-c, IPC-1-SnPI and Sn-MS were examined using *in-situ* pyridine adsorption followed by FT-IR analysis. After activation at 450°C under vacuum, all samples exhibited a sharp band at 3745 cm^{-1}, characteristic for terminal silanol groups [28] (Figure S4, supporting information). No other bands were observed in the region of O-H vibrations. After pyridine adsorption and subsequent desorption at 150°C under vacuum (15 min), characteristic bands for pyridine coordinated to Lewis acid site were observed at 1454 cm^{-1} together with a band at 1490 cm^{-1} [28] (combination of pyridine on Lewis acid site and pyridine on Bronsted acid site; Figure S4, supporting information). No band at 1545 cm^{-1} was observed evidencing the absence Bronsted acid sites in Sn samples. The area of the band at 1454 cm^{-1} (A_L) increased with increasing Sn content: **MFI**-SnPI-c (Si/Sn=44, A_L=3.041) < IPC-1-SnPI (Si/Sn=32, A_L=3.204) < Sn-MS (Si/Sn=17, A_L=4.393). After desorption at 250°C (15 min), the intensity of the bands decreased considerably (e.g. A_L (Sn-MS, 250°C) = 0.604) showing low acid strength of Lewis acid sites. After 15 min desorption at 450°C, all pyridine was removed from the catalyst surface.

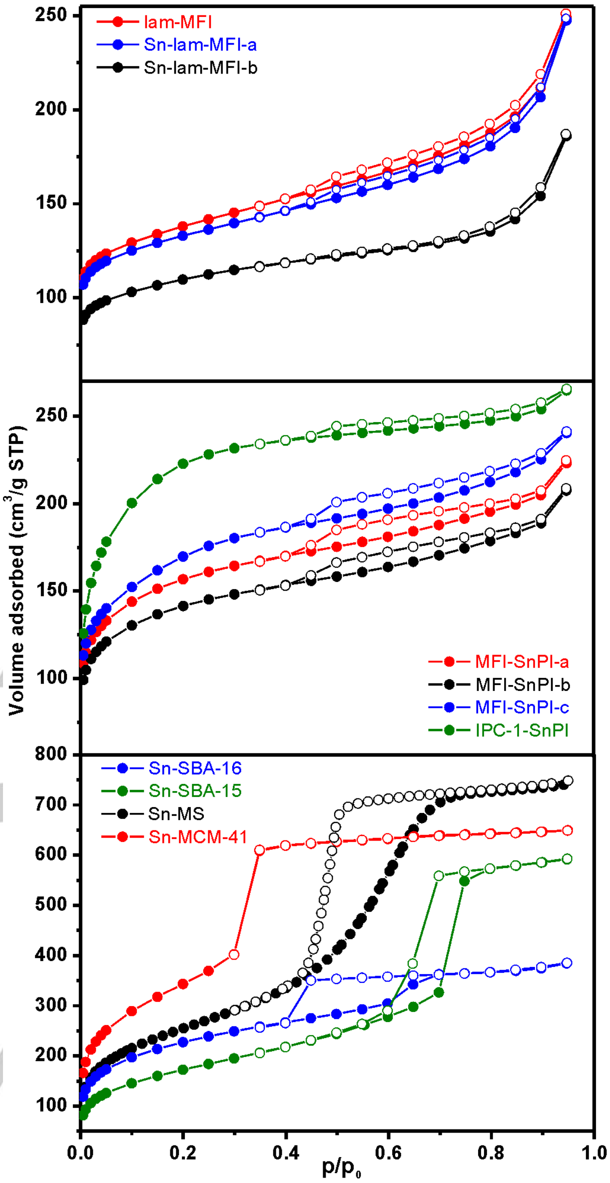

Figure 4. Adsorption-desorption N_2 isotherms collected at -196°C for the discussed catalysts. Empty points denote desorption.

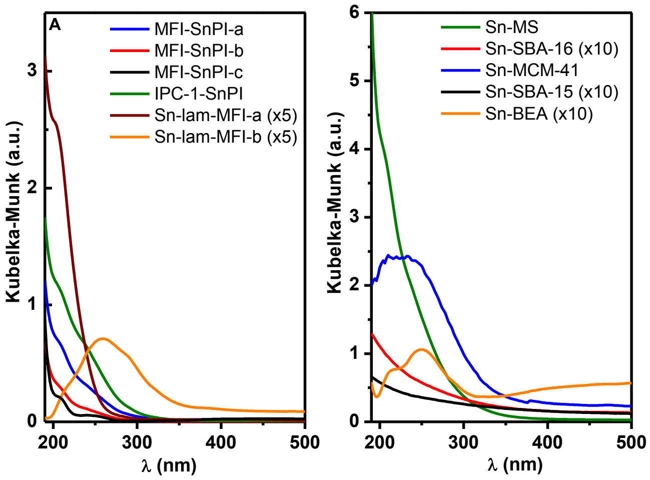

Figure 5. DR-UV/Vis spectra of lamellar and pillared tin materials (A) and tin mesoporous silica catalysts and Sn-**BEA** (B).

Catalytic testing

Norcamphor, 2-adamantanone, and cyclopentanone were tested in Baeyer-Villiger oxidation using the tin containing catalysts with H_2O_2 as the oxidant at 80°C (Figure 6). Table 2 summarizes the results of the oxidation of norcamphor. In order to confirm the activity of the catalysts, blank experiment was carried out under the same conditions like for all other experiments. No conversion of norcamphor was detected during 24 h.

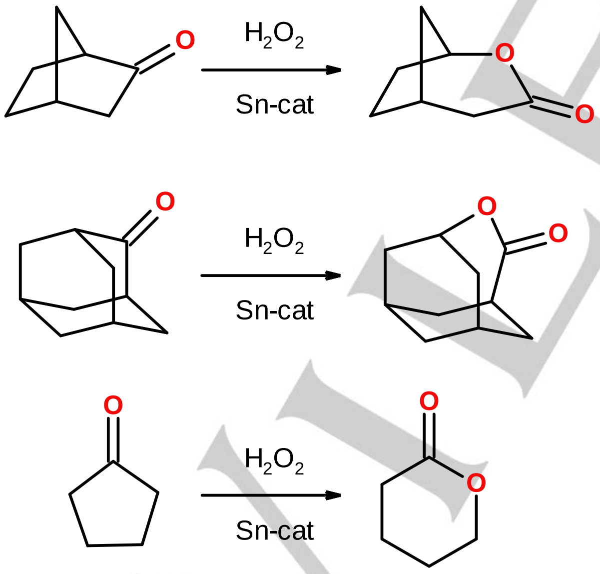

Figure 6. Reaction schemes for Baeyer-Villiger oxidation of norcamphor (top), 2-adamantanone (middle) and cyclopentanone (bottom).

The highest norcamphor conversions were observed using mesoporous Sn-MS prepared by direct synthesis (37% after 8 h) and tin-silica pillared IPC-1-SnPI (36% after 8 h). The order of the mesoporous catalysts in terms of conversion after 8 h was Sn-MS > Sn-MCM-41(22%) > Sn-SBA-15 (16%) > Sn-SBA-16 (7%). Norcamphor conversions over the pillared **MFI** catalysts after 8 h are comparable with these provided by Sn-MCM-41 and Sn-SBA-15 (**MFI**-SnPI-a: 14%, **MFI**-SnPI-b: 11%, **MFI**-SnPI-a: 20% vs. Sn-SBA-15: 16%, Sn-MCM-41: 22%). Sn-**BEA** also fits to this group of catalysts providing 13% conversion at the same time.

Table 2. Baeyer-Villiger oxidation of norcamphor with H_2O_2 over different catalysts at 80°C; conversion, TON and selectivity to the lactone after 8 h of the reaction.

Catalyst	Conversion (%)	TON	Selectivity lactone (%)
Blank	0		0
Sn-lam-MFI-a	0.6	2	n.d.
Sn-lam-MFI-b	1.6	1	n.d.
MFI-SnPI-a	14	6	93
MFI-SnPI-b	11	8	>99
MFI-SnPI-c	20	21	95
IPC-1-SnPI	36	28	93
Sn-SBA-16	7	9	>99
Sn-SBA-15	16	16	94
Sn-MS	37	15	89
Sn-MCM-41	22	26	99
Sn-BEA	13	69	95

Reaction conditions: 50 mg of catalyst, 2 mmol norcamphor, 2 mmol H_2O_2 (35%wt aqueous sol.), 80ºC, 6 ml 1,4-dioxane, 8 h.

Selectivity to lactone in Baeyer-Villiger oxidation of norcamphor was higher than 99% at 10% conversion for all the mesoporous catalysts but later on it started to drop. The Sn-MS provided selectivity 89% at 40% conversion, Sn-MCM-41 74% and Sn-SBA-15 61% at this conversion.

It should be noted that the Sn-MS catalyst exhibited selectivity of 87% even at 80% conversion and the only other catalyst providing conversion over 50% within 24 h was IPC-1-SnPI, giving 53% conversion with 76% selectivity. The high conversion observed for the Sn-MS catalyst can be attributed to the tetrahedral coordination of tin in this catalyst connected with a good accessibility of the active centres due to its high BET area (920 m^2/g), high adsorption volume (1.17 cm^3/g) and mesoporous sponge-like morphology (*vide supra*).

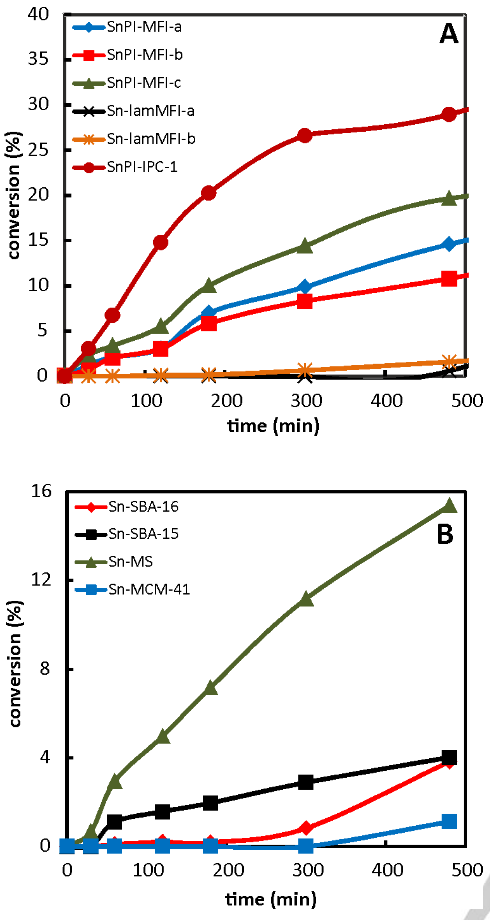

Figure 7. Conversion of norcamphor in time using lamellar and pillared tin-catalysts (A) and tin mesoporous molecular sieves (B). Reaction conditions: 50 mg of catalyst, 2 mmol norcamphor, 2 mmol H_2O_2 (35%wt aqueous sol.), 80ºC, 6 ml 1,4-dioxane.

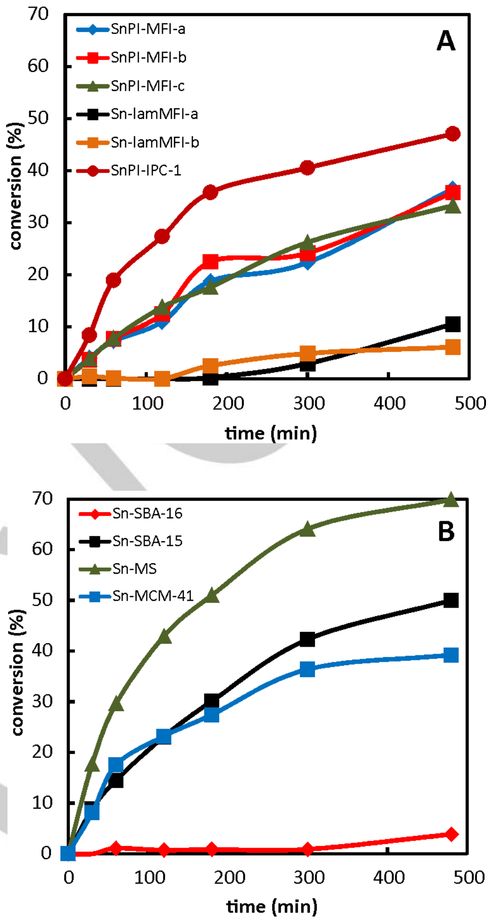

Figure 8. Conversion of 2-adamantanone in time using lamellar and pillared tin-catalysts (A) and tin mesoporous molecular sieves (B). Reaction conditions: 50 mg catalyst, 2 mmol 2-adamantanone, 2 mmol H_2O_2 (35%wt aqueous sol.), 80°C, 6 ml 1,4-dioxane.

Among the crystalline lamellar catalysts the IPC-1-SnPI gave the highest conversion (36% after 8 h) with 93% selectivity at 36% conversion. It was also the second most active in terms of turn-over-number (TON = 28, mol converted/mol Sn after 8 h) after Sn-**BEA** (TON = 69 after 8 h). Regarding the pillared **MFI** based catalysts, the observed TONs are proportional to the Si/Sn ratio (compare Table 1 and Table 2). This shows that full intrinsic activity of the active sites cannot manifest itself (compare also with Sn-**BEA** (Si/Sn = 220, TON = 69). If the reaction system was in a kinetic regime, the TON (which is calculated per Sn atom) should be the same as long as sufficient amount of reactants is available (and all SnPI-MFI catalysts have similar Sn species distribution - see UV/Vis spectra in figure 5). But this is not the case and therefore, we conclude the reaction is mainly diffusion driven. Despite the high Sn content (Si/Sn=27), the $SnCl_4$ impregnated Sn-lam-**MFI**-b provided conversion only 1.6 % after 8 h because most of tin is present in the form of SnO_2 and the SnO_2 phase is catalytically inactive for the studied reaction. [7b] Full conversion profiles are presented in Figure 7.

2-adamantanone is more reactive than norcamphor because it possesses two tertiary carbon atoms adjacent to the carbonyl group. Nevertheless, it does not undergo oxidation without a catalyst. Conversion, selectivity and TON obtained with the discussed catalysts after 8 h of reaction are listed in Table 3. Full conversion curves are presented in Figure 8.

The highest 2-adamantanone conversion (70% after 8 h) was achieved again using Sn-MS. The order of the 2-adamantanone conversions after 8 h was following: Sn-MS (70%) > Sn-SBA-15 (50%) ≈ IPC-1-SnPI (47%) > Sn-MCM-41 (36%) ≈ **MFI**-SnPI-a,b,c (36%, 36%, 33%, respectively) > Sn-SBA-16 (24%) > Sn-lam-**MFI**-a (10%) > Sn-lam-**MFI**-b (6%). Interestingly, the differences in conversion between tin-silica pillared **MFI** catalysts, which were observed in oxidation of norcamphor, practically disappeared (Figure 8A).

Table 3. Baeyer-Villiger oxidation of 2-adamantanone with H_2O_2 over different catalysts at 80°C; conversion, TON and selectivity to the lactone after 8 h of the reaction.

Catalyst	Conversion (%)	TON	Selectivity lactone (%)
Blank	0	--	0
Sn-lam-MFI-a	10	37	34
Sn-lam-MFI-b	6	4	92
MFI-SnPI-a	36	16	75
MFI-SnPI-b	36	26	77
MFI-SnPI-c	33	35	88
IPC-1-SnPI	47	36	96
Sn-SBA-16	24	31	>99
Sn-SBA-15	50	49	92
Sn-MS	70	29	>99
Sn-MCM-41	36	43	84
Sn-BEA	13	69	75

Reaction conditions: 50 mg of catalyst, 2 mmol 2-adamantanone, 2 mmol H_2O_2 (35%wt aqueous sol.), 80ºC, 6 ml 1,4-dioxane, 8 h.

The order of 2-adamantanone conversion over different catalysts follows with some exceptions the order of the catalysts in terms of total adsorption volume (e.g. Sn-MS: Vtot=1.17 cm^3/g > Sn-SBA-15: Vtot=1.10 cm^3/g > **MFI**-SnPI-a: Vtot=0.35 cm^3/g , cf. Table 1). One would expect Sn-MCM-41 to achieve 2-adamantanone conversion at least similar to Sn-SBA-15, but this is not the case and Sn-MCM-41 fits in terms of both conversion and selectivity to the group of **MFI**-SnPI-a, **MFI**-SnPI-b and **MFI**-SnPI-c (selectivity between 75 and 88% at 36% conversion). We ascribe this behaviour to different distribution of Sn species in comparison with Sn-SBA-15 (cf. Figure 5). On the other hand, IPC-1-SnPI provided conversion similar to Sn-SBA-15. It is also the most active (TON=36 after 8 h) and selective (96% at 50% conversion) of the catalysts with crystalline layers. This is because the IPC-1-SnPI possesses combination of the advantages of a well ordered crystalline zeolitic structure together with accessibility of the active sites similar to mesoporous silica materials. Sn-**BEA** provided only 13% conversion after 8 h because of its low Sn content (Si/Sn = 220) but, like in the case of norcamphor, it provided the highest TON (69 after 8 h).

It has been mentioned that the Baeyer-Villiger reaction proceeds via 2 step mechanism (nucleophilic attack of the peroxide specie and subsequent migration of adjacent carbon atom). [3] Since in the 2-adamantanone molecule, the tertiary carbon atoms can easily migrate, [6] polarization of the carbonyl group by the Sn-center should significantly favor the Baeyer-Villiger oxidation against other transformations. However, only some of the catalysts (Sn-MS, Sn-SBA-15, IPC-1-SnPI, and Sn-SBA-16; interestingly those giving the highest conversion) provided selectivity over 90% at 50% conversion.

The Sn-MS catalyst exhibited selectivity to the lactone over 99% even at 70% conversion; however, rationalization of the observed selectivity data is a complex issue. Among the mesoporous molecular sieves, the selectivity can be correlated with distribution of Sn species (cf. Figure 5). Lack of absorption band at about 250 nm corresponds to higher selectivity (>99% at 30% conversion (SBA-16, Sn-MS) vs. 84% Sn-MCM-41).

In the group of layered zeolite catalysts, the IPC-1-SnPI fits to the above rule; however, the layered and pillared **MFI** catalysts provided generally lower selectivity (75-88% at 30% conversion). It appears that the selectivity is very sensitive to local environment of the active site and not only to Sn coordination state.

In contrast to norcamphor and 2-adamantanone, cyclopentanone is a sterically less demanding molecule and therefore smaller differences between micro-mesoporous SnPI-**MFI** catalysts and purely mesoporous catalysts were expected. The results of the cyclopentanone oxidation confirmed this expectation (Table 4). Conversion profiles are presented in Figure 9. **MFI**-SnPI-a, **MFI**-SnPI-b and **MFI**-SnPI-c gave conversions 13%, 7% and 10%, respectively, after 8 h. Only the Sn-MS provided higher conversion (15%) at the same time (8 h). Sn-lam-**MFI**-b and Sn-MCM-41 catalysts were practically inactive. The reason is not completely clear but we assume it is connected to presence of SnO_2 which is the main difference in comparison with other catalysts (note the differences in the DR-UV/Vis spectra among individual catalysts (Figure 5)). We conclude the Baeyer-Villiger oxidation of cyclopentanone appears to be more difficult in comparison with norcamphor and 2-adamantanone. The reason can be that the secondary carbon atoms adjacent to the carbonyl group in cyclopentanone migrate less easily than tertiary atoms in the other two substrates[6].

Also the selectivity to γ-valerolactone in the cyclopentanone oxidation was lower in comparison with norcamphor and 2-adamantanone, because γ-valerolactone, formed in the Baeyer-Villiger oxidation of cyclopentanone, easily undergoes hydrolysis to corresponding hydroxyacid. [29]

The highest selectivity was observed using **MFI**-SnPI-b (57% at 5% conversion) but the selectivities of other active catalysts (MFI-SnPI-c, Sn-SBA-15, Sn-SBA-16, Sn-MS) did not differ much (ranging from 46 to 55% at 5% conversion, Table 4). It should be noted that Sn-lam-**MFI**-a and **MFI**-SnPI-c provided the same TON as Sn-**BEA** (11 after 8 h).

To verify the stability against regeneration, **MFI**-SnPI-a, IPC-1-SnPI and Sn-MS were collected after the reaction, washed with methanol, dried and recalcined at 500°C to remove any organic residues. After this regeneration, XRD pattern and UV/Vis spetra were collected and compared with the fresh catalysts (Figure S5 S6, supporting information). No significant changes were observed and therefore, we conclude the materials did not undergo any significant change during the catalytic experiment.

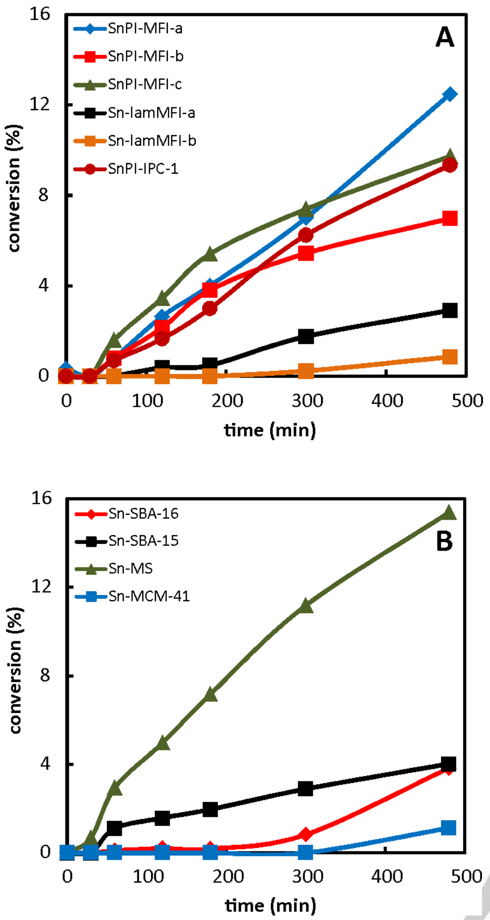

Figure 9. Time dependence of conversion of cyclopentanone over lamellar and pillared tin-catalysts (A) and tin mesoporous molecular sieves (B). Reaction conditions: 50 mg catalyst, 2 mmol cyclopentanone, 1mmol H_2O_2 (35%wt aqueous sol.), 80ºC, 1,4-dioxane.

Table 4. Baeyer-Villiger oxidation of cyclopentanone with H_2O_2 over different catalysts at 80°C; conversion, TON and selectivity to the lactone after 8 h of the reaction.

Catalyst	Conversion (%)	TON	Selectivity lactone (%)
Blank	0	--	0
Sn-lam-MFI-a	2.9	11	28
Sn-lam-MFI-b	<1	1	n.d.
MFI-SnPI-a	13	6	31
MFI-SnPI-b	7	5	57
MFI-SnPI-c	10	11	50
IPC-1-SnPI	9	7	34
Sn-SBA-16	4	5	46
Sn-SBA-15	4	4	50
Sn-MS	15	6	55
Sn-MCM-41	<1	1	n.d.
Sn-BEA	2	11	n.d.

Reaction conditions: 50 mg catalyst, 2 mmol cyclopentanone, 1mmol H_2O_2 (35%wt aqueous sol.), 80ºC, 1,4-dioxane, 8h.

Conclusions

We report the synthesis and catalytic properties of a set of novel tin-silica molecular sieve catalysts in Baeyer-Villiger oxidation with hydrogen peroxide. Layered **MFI** based Sn-silicate catalysts were prepared by impregnation of pure silica **MFI** nanosheets and by their tin-silica pillaring. Ordered mesoporous silica catalysts Sn-SBA-15, Sn-SBA-16 and Sn-MCM-41 were prepared by impregnation with $SnCl_4$ and a new Sn-MS material was formed by direct synthesis in the presence of diquaternary ammonium surfactant $C_{18\text{-}6\text{-}6}OH_2$. In addition, tin-silica pillared IPC-1 material was obtained by top-down transformation of **UTL** zeolite and subsequent swelling and tin-silica pillaring.

These catalysts were active in Baeyer-Villiger oxidation of norcamphor, 2-adamantanone, and cyclopentanone. Norcamphor and 2-adamantanone were oxidized easily with selectivity up to 99%. Sn-MS and IPC-1-SnPI materials provided the highest conversions of these two substrates (norcamphor conversion 37% resp. 36%, 2-adamandanone conversion 70% resp. 47% after 8 h). Structurally similar SnPI-**MFI** catalysts with different Sn content provided very similar conversions. Especially in the case of bulky 2-adamantanone, the conversion was independent on Sn content for the SnPI-**MFI** catalysts. This shows an important role of accessibility of the active sites in determining the catalyst activity. Although the Sn-**BEA** catalyst exhibited higher TON in oxidation of norcamphor and 2-adamantanone, the advantage of the new catalysts remains in their fast and facile preparation and higher Sn content and therefore higher yield of the desired product. On the other hand, cyclopentanone, although being less sterically demanding, was found difficult to oxidise and the reactions suffered from product hydrolysis to corresponding 4-hydroxybutanoic acid. As a result, conversion only up to 15% after 8 h and selectivity only up to 57% at 5% conversion was observed. One more time Sn-MS provided the highest conversion, followed by SnPI-**MFI** catalysts.

Experimental Section

Parent lamellar pure silica **MFI** material was synthesized using the procedure originally described by Na et al. [10b] 0.0637 mol of tetraethyl orthosilicate (TEOS, Aldrich) was hydrolyzed in a solution of 0.0038 mol of structure directing agent (SDA) $C_{18}H_{37}$ -$N^+(CH_3)_2$ -C_6H_{12} -$N^+(CH_3)_2$ -C_6H_{13} in hydroxide form ($C_{18\text{-}6\text{-}6}OH_2$; prepared according to the literature[10b]) in distilled water (65 ml). The synthesis gel with initial composition 100 TEOS: 6 $C_{18\text{-}6\text{-}6}OH_2$: 5000 H_2O was homogenized at 60°C for 3 h. The evaporated weight of ethanol and water was replaced with the same amount of water at the end. The hydrothermal crystallization took place in a 90 ml Teflon-lined autoclave at 155°C for 240 h under agitation. After the given time, the zeolite was filtered off, washed out with water, dried at 65°C and finally calcined or subjected to the tin-silica pillaring treatment. Calcination was carried out at 550°C for 6 h, using a temperature ramp of 2°C/min.

The tin-silica pillared catalysts were prepared from as-synthesized parent lamellar all-silica **MFI**. 1 g of dry parent material was dispersed in a mixture of 10 g of TEOS and 464 mg of tin (IV) butoxide (Aldrich; Si/Sn molar ratio 40 (**MFI**-SnPI-a) or 10 of TEOS and 4 ml (**MFI**-SnPI-b) resp. 2 ml (**MFI**-SnPI-c) of Sn(IV) isopropoxide 25 wt.% solution in 2-propanol

(Aldrich) . The mixtures were stirred at 65°C for 24 h. Then, the mixtures were centrifuged and the solid materials were dried for 48 h at room temperature. Individual samples were hydrolyzed in water with 5% of ethanol (100 ml/1 g) at ambient temperature for 24 h under vigorous stirring. Finally, the materials were centrifuged again, dried at 65°C and calcined in air, at 550° C for 10 h, using the temperature ramp of 2° C/min.

IPC-1-SnPI material was prepared from parent **UTL** zeolite. Synthesis procedure of the B-**UTL**, procedure for the B-**UTL** disassembly into IPC-1P lamellar precursor and swelling procedure forming IPC-1SW material were the same as in ref. [13-14, 17] Swollen IPC-1SW (consisting of silica IPC-1 layers with intercalated cetyltrimethylammonium hydroxide surfactant) was tin-silica pillared with a mixture of TEOS and Sn(IV) butoxide using the above procedure for **MFI**-SnPI-a. Final hydrolyzed material was calcined with a temperature program of 200°C for 2 h, then 350°C for 4 h and finally 550°C for 8h, using a temperature ramp of 2°C/min.

Impregnation of the pure silica supports with Sn(IV) chloride ($SnCl_4$, Aldrich, 98%) was performed using the following procedure. $SnCl_4$ was dissolved in dry toluene. The parent support (pure silica layered **MFI**, SBA-15, SBA-16 or MCM-41) was activated at 450°C for 60 min, cooled down in a desiccator and added to the $SnCl_4$ solution. The mixture was stirred at room temperature for 16 h in a glass round bottom flask under nitrogen atmosphere. In particular, 217 mg of $SnCl_4$ and 15 ml of toluene were used per 0.5 g of the parent material. After the given time, the mixture was centrifuged, washed out with fresh dry toluene and the impregnated zeolite was dried at 65°C. At the end, the material was calcined at 550°C for 6 h with the temperature ramp of 2°C/min.

Impregnation of the supports with Sn(IV) butoxide was carried out using a similar procedure. Sn(IV) butoxide was dissolved in 1-butanol and the activated parent material (pure silica layered **MFI**) was introduced into the mixture. The mixture was stirred and heated at 50°C for 16 h in a glass round bottom flask under nitrogen atmosphere. In particular, 35 mg of Sn(IV) butoxide and 15 ml of 1-butanol were used per 0.5 g of the parent material. After the given time, the mixture was centrifuged, two times washed out with fresh 1-butanol and the impregnated zeolite was dried at 65°C and calcined at 550°C for 6 h with the temperature ramp of 2°C/min.

The Sn-MS material was synthesized from 2 mmol of $SnCl_4.5\ H_2O$ and 100 mmol of TEOS using 35 mmol of SDA $C_{18\text{-}6\text{-}6}OH_2$ (*vide supra*). The $SnCl_4.5\ H_2O$ was dissolved in a solution of SDA in 4 mol of distilled water. Then, the TEOS was added and the mixture was homogenized at room temperature for 1 h. Final gel was hydrothermally treated for 260 h at 160°C. After the given time, the product was filtered off, washed with water, dried at 65°C and calcined at 550°C for 8 h with a temperature ramp of 2°C/min.

The structure and crystallinity of the samples were determined by X-ray powder diffraction using a Bruker AXS D8 Advance diffractometer equipped with a graphite monochromator and position-sensitive detector Våntec-1 using Cu Kα radiation in Bragg–Brentano geometry. The crystalline samples (lamellar and pillared) were measured in 2θ range 1-40°. XRD patterns of mesoporous sieves were recorded using 2θ range 0.75-10°.

Textural properties were determined from nitrogen adsorption/desorption isotherms recorded on a Micromeritics ASAP2020 volumetric instrument at -196°C. Prior to the measurement, individual samples were degassed in a stream of helium at 300°C for 3 h. The BET area was determined from adsorption data in the range of a relative pressure from P/P_0= 0.05 to P/P_0 =0.20. [30] The micropore volume (V_{mic}) and external surface area (S_{ext}) were determined by t-plot method. [31] Total adsorption volume (V_{tot}) was determined from nitrogen amount adsorbed at relative pressure P/P_0= 0.95.

Diffuse reflectance ultraviolet-visible (DR-UV/Vis) spectra were obtained using Perkin-Elmer Lambda 950 Spectrometer with a 2 mm quartz tube and a 8 x 8 mm slit. Spectra were collected in a wavelength range of 190-500 nm with a 100% reflectance standard ($BaSO_4$), and converted to an absorption spectrum using the Kubelka-Munk function.

The content of Sn was determined using an ICP-OES ThermoScientific iCAP 7000 instrument. The samples (50mg) were dissolved in a mixture of 4 ml of HCl (36 %), 4 ml of HNO_3 (67 %) and 2 ml of HF (48 %). The solution was treated in the microwave irradiation and subsequently 15ml of H_3BO_3 was added to complex the HF excess. Finally the solutions were diluted by ultrapure water.

Morphological characterization was carried out by scanning electron microscopy technique (SEM) on a JEOL, JSM-5500LV microscope. The images were collected with an acceleration voltage of 20 kV.

The Baeyer-Villiger oxidation was investigated in a 25 ml magnetically stirred glass two-necked round bottom flask equipped with a reflux condenser at 80°C. Prior to the catalytic experiment catalyst was activated in air at 450°C for 90 min and let to cool down in a desiccator. In a typical experiment, catalyst powder 50 mg, was added to a solution consisting of 2 mmol of the ketone (cyclopentanone (Aldrich), norcamphor (Aldrich) or 2-adamantanone (Aldrich)), 1.08 mmol mesitylene (internal standard) and 6 ml of 1,4-dioxane. The reaction was started by addition of 2 mmol of H_2O_2 (Aldrich, 35 wt% aqueous solution, 1 molar equivalent). Therefore, maximum theoretical conversion was 100%. In case of cyclopentanone, 1 mmol of H_2O_2 (0.5 molar equivalents) was used. Samples of the reaction mixture were taken in regular interval, centrifuged to remove the catalyst and analyzed using an Agilent 6850 gas chromatograph with a 50 m long DB-5 column an autosampler and FID detector.

Acknowledgements

The authors acknowledge the Czech Science Foundation (P106/12/G015) for the financial support of this research.

Keywords: Heterogeneous catalysis • Ketones • Layered zeolite • Oxidation • Tin-silicate

[1] A. Baeyer, V. Villiger, *Chem. Ber.* **1899**, *32*, 3625-3633.
[2] C. Jiménez-Sanchidrián, J. R. Ruiz, *Tetrahedron* **2008**, *64*, 2011-2026.
[3] R. Criegge, *Justus Liebigs Ann. Chem.* **1948**, *560*, 127.
[4] R. A. Michelin, P. Sgarbossa, A. Scarso, G. Strukul, *Coord. Chem. Rev.* **2010**, *254*, 646-660.
[5] M. Renz, B. Meunier, *Eur. J. Org. Chem.* **1999**, *1999*, 737-750.
[6] G. J. ten Brink, I. W. C. E. Arends, R. A. Sheldon, *Chem. Rev.* **2004**, *104*, 4105-4124.
[7] a) A. Corma, L. T. Nemeth, M. Renz, S. Valencia, *Nature* **2001**, *412*, 423-425; b) M. Renz, T. Blasco, A. Corma, V. Fornés, R. Jensen, L. Nemeth, *Chem. Eur. J.* **2002**, *8*, 4708-4717; c) A. Corma, M. a. T. Navarro, M. Renz, *J. Catal.* **2003**, *219*, 242-246; d) I. Nowak, A. Feliczak, I. Nekoksová, J. Čejka, *Appl. Catal., A* **2007**, *321*, 40-48; e) I. Nekoksová, N. Žilková, J. Čejka, in *Stud. Surf. Sci. Catal., Vol. 158 B*

(Eds.: J. Čejka, N. Žilková, P. Nachtigall), Elsevier, **2005**, pp. 1589-1596; f) H. Xu, J. Jiang, B. Yang, H. Wu, P. Wu, *Catal. Commun.* **2014**, *55*, 83-86.

[8] a) M. Del Todesco Frisone, F. Pinna, G. Strukul, *Organometallics* **1993**, *12*, 148-156; b) S. Shambayati, S. L. Schreiber, in *Comprehensive Organic Synthesis, Vol. 1* (Eds.: B. M. Trost, I. Fleming), Pergamon, Oxford, **1991**, pp. 283-324.

[9] H. Y. Luo, L. Bui, W. R. Gunther, E. Min, Y. Román-Leshkov, *ACS Catal.* **2012**, *2*, 2695-2699.

[10] a) W. J. Roth, P. Nachtigall, R. E. Morris, J. Čejka, *Chem. Rev.* **2014**, *114*, 4807-4837; b) K. Na, C. Jo, J. Kun, W. S. Ahn, R. Ryoo, *ACS Catal.* **2011**, *1*, 901-907; c) J. Přech, P. Eliášová, D. Aldhayan, M. Kubů, *Catal. Today* **2015**, *243*, 134-140.

[11] S. Conrad, P. Wolf, P. Müller, H. Orsted, I. Hermans, *ChemCatChem* **2017,** *9*, 175-182.

[12] A. Al-Nayili, K. Yakabi, C. Hammond, *J. Mater. Chem. A,* **2016**,*4*, 1373-1382.

[13] M. V. Opanasenko, W. J. Roth, J. Cejka, *Catal. Sci. Technol.* **2016**, *6*, 2467-2484.

[14] L. Ren, Q. Guo, P. Kumar, M. Orazov, D. Xu, S. M. Alhassan, K. A. Mkhoyan, M. E. Davis, M. Tsapatsis, *Angew. Chem., Int. Ed.* **2015**, *54*, 10848-10851.

[15] J. Přech, J. Čejka, *Catal. Today* **2016**, *277*, 2-8.

[16] W. J. Roth, O. V. Shvets, M. Shamzhy, P. Chlubná, M. Kubů, P. Nachtigall, J. Čejka, *J. Am. Chem. Soc.* **2011**, *133*, 6130-6133.

[17] M. Choi, K. Na, J. Kim, Y. Sakamoto, O. Terasaki, R. Ryoo, *Nature* **2009**, *461*, 828-828.

[18] a) W. J. Roth, J. Čejka, *Catal. Sci. Technol.* **2011**, *1*, 43-53; b) P. Eliášová, M. Opanasenko, P.S. Wheatley, M. Shamzhy, M. Mazur, P. Nachtigall, W. J. Roth, R. E. Morris, J. Čejka, Chem. Soc. Rev. 2015, 44, 7177-7206.

[19] M. Mazur, P. S. Wheatley, M. Navarro, W. J. Roth, M. Položij, A. Mayoral, P. Eliášová, P. Nachtigall, J. Čejka, R. E. Morris, *Nat. Chem.* **2016**, *8*, 58-62.

[20] K. Na, M. Choi, W. Park, Y. Sakamoto, O. Terasaki, R. Ryoo, *J. Am. Chem. Soc.* **2010**, *132*, 4169-4177.

[21] J. S. Beck, J. C. Vartuli, W. J. Roth, M. E. Leonowicz, C. T. Kresge, K. D. Schmitt, C. T. W. Chu, D. H. Olson, E. W. Sheppard, S. B. McCullen, J. B. Higgins, J. L. Schlenker, *J. Am. Chem. Soc.* **1992**, *114*, 10834-10843.

[22] D. Zhao, Q. Huo, J. Feng, B. F. Chmelka, G. D. Stucky, *J. Am. Chem. Soc.* **1998**, *120*, 6024-6036.

[23] M. Mesa, L. Sierra, J. Patarin, J.-L. Guth, *Solid State Sci.* **2005**, *7*, 990-997.

[24] P. I. Ravikovitch, A. V. Neimark, *Langmuir* **2002**, *18*, 1550-1560.

[25] M. Moliner, Y. Román-Leshkov, M. E. Davis, *Proc. Natl. Acad. Sci. U. S. A.* **2010**, *107*, 6164-6168.

[26] J. W. Harris, M. J. Cordon, J. R. Di Iorio, J. C. Vega-Vila, F. H. Ribeiro, R. Gounder, *J. Catal.* **2016**, *335*, 141-154.

[27] K. Chaudhari, T. K. Das, P. R. Rajmohanan, K. Lazar, S. Sivasanker, A. J. Chandwadkar, *J. Catal.* **1999**, *183*, 281-291.

[28] B. Gil, S. I. Zones, S.-J. Hwang, M. Bejblová, J. Čejka *J. Phys. Chem. C* **2008**, 112, 2997-3007.

[29] A. Drożdż, A. Chrobok, S. Baj, K. Szymańska, J. Mrowiec-Białoń, A. B. Jarzębski, *Appl. Catal., A* **2013**, *467*, 163-170.

[30] S. Brunauer, P. H. Emmett, E. Teller, *J. Am. Chem. Soc.* **1938**, *60*, 309-319.

[31] B. C. Lippens, J. H. de Boer, *J. Catal.* **1965**, *4*, 319-323.

10.1002/cctc.201700162

Entry for the Table of Contents (Please choose one layout)

Layout 1:

FULL PAPER

Text for Table of Contents

((Insert TOC Graphic here: max. width: 5.5 cm; max. height: 5.0 cm))

*Author(s), Corresponding Author(s)**

Page No. – Page No.

Title

Layout 2:

FULL PAPER

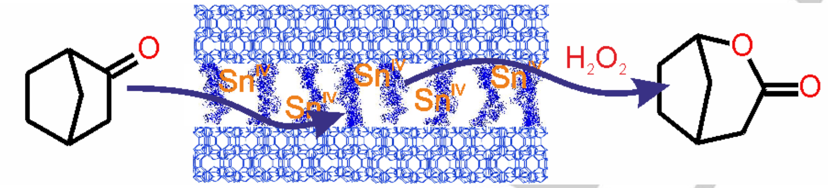

The tin-silica pillaring of a layered zeolite enables to prepare a tin containing catalyst, which combines the advantages of crystalline zeolite and mesoporous molecular sieve. The tin-silica pillared zeolites catalyse Baeyer-Villiger oxidation of cyclic ketones with aqueous hydrogen peroxide.

Jan Přech, Marta Arroyo Carretero, Jiří Čejka*

Page No. – Page No.

Baeyer-Villiger oxidation of cyclic ketones using tin-silica pillared catalysts